Atmos. Meas. Tech. Discuss., 7, 9733–9769, 2014
www.atmos-meas-tech-discuss.net/7/9733/2014/
doi:10.5194/amtd-7-9733-2014

Atmospheric Measurement Techniques Discussions
Open Access

Differences in aerosol absorption Ångström exponents between correction algorithms for particle soot absorption photometer measured on South African Highveld

J. Backman[1], A. Virkkula[1,2], V. Vakkari[1], J. P. Beukes[3], P. Van Zyl[3], M. Josipovic[3], S. Piketh[3], P. Tiitta[3,4], K. Chiloane[5,6], T. Petäjä[1], M. Kulmala[1], and L. Laakso[2,3]

[1]Department of Physics, University of Helsinki, Helsinki, Finland
[2]Finnish Meteorological Institute, Helsinki, Finland
[3]School of Physical and Chemical Sciences, North-West University, Potchefstroom, Republic of South Africa
[4]Department of Environmental Science, University of Eastern Finland, Kuopio, Finland
[5]Unit for Environmental Sciences and Management, North-West University, Potchefstroom, Republic of South Africa
[6]Eskom Holdings SOC Ltd, Sustainability Division, Research, Testing and Development, South Africa

Received: 30 June 2014 – Accepted: 31 August 2014 – Published: 19 September 2014

Correspondence to: J. Backman (john.backman@helsinki.fi)

Published by Copernicus Publications on behalf of the European Geosciences Union.

AMTD
7, 9733–9769, 2014

Abstract

Absorption Ångstrom exponents (AAE) calculated from filter-based absorption measurements are often used to give information on the origin of the ambient aerosol, for example to distinguish between urban pollution and biomass burning aerosol. Filter-based absorption measurements are a widely used method and are commonly used at aerosol monitoring stations globally. Several correction algorithms are used to account for the artifacts associated with filter-based absorption techniques. These algorithms are of profound importance when determining the absolute amount of absorption by the aerosol. However, this study shows that there are significant differences between the AAEs calculated from these corrections. The study also shows that the difference between AAEs calculated using different corrections can lead to conflicting conclusions on the type of aerosol for the same data set. In this work the AAEs were calculated from data measured with a three-wavelength Particle Soot Absorption Photometer (PSAP) at Elandsfontein on deployed on the South African Highveld for 23 months. The sample air of the PSAP was diluted to prolong filter change intervals. The dilution-corrected PSAP showed a good agreement with a non-diluted MAAP. Thus, the study also shows that the applicability of the PSAP can be extended to remote sites are not often visited or suffer from high levels of pollution.

1 Introduction

Atmospheric aerosols form part of the climatic system of the Earth. Aerosol light scattering, absorption, or both, will reduce solar insolation at the surface and alter the radiative transfer through the atmosphere. This is called the “direct radiative effect” of aerosols (Haywood and Boucher, 2000; Lohmann and Feichter, 2005). A strong light absorbing particle specie is black carbon (BC) which is a byproduct of incomplete combustion processes. A study by Bond et al. (2013) concluded that BC is the second most important positive radiative forcer. In this study, the term BC will be used according to

AMTD
7, 9733–9769, 2014

the definition by Bond et al. (2013), i.e. a material with specific properties. BC particles are made of spherules of mostly pure carbon that form aggregates. They absorb solar radiation with a weak spectral selectivity and are therefore black by appearance (Kirchstetter et al., 2004; Andreae and Gelencser, 2006). However, not all light absorbing particles are black by appearance. Certain organic carbon (OC) containing aerosols have been shown to exhibit a spectral selectivity that exceeds that of BC particles. These particles are called brown carbon (BrC) since they appear brownish to the eye and strongly absorbs light at shorter wavelengths. BrC is a known constituent of biomass burning aerosol (Kirchstetter et al., 2004). In addition, desert dust is a major constituent of total suspended particle mass also absorbs light at short wavelengths.

The extent to which light interacts with aerosol particles can be expressed by the scattering coefficient (σ_{SP}), absorption coefficient (σ_{AP}), and the extinction coefficient σ_{EP}. The spectral dependency light interaction can be described by the Ångström exponent (AE). By convention, AE is the negative slope of the wavelength dependency of the above coefficients in logarithmic space

$$\ln(\sigma_i(\lambda_i)) = -\mathrm{AE}\ln(\lambda_i) + C, \quad (1)$$

where σ_i is the scattering, absorption or extinction coefficient at wavelength λ_i. When substituting σ_i with σ_{AP} in Eq. (1), AE will represent the light absorption Ångström exponent (AAE). Thus, AAE describes the spectral dependence of light absorption by the aerosol. The work by Moosmüller et al. (2011) provides a more in-depth view of its definition. When σ_i is the substituted with σ_{SP}, AE becomes the scattering Ångström exponent (SAE).

The wavelength dependency of light scattering and absorption is not only of climatic importance, but can also provide additional information on the aerosol size distribution and chemical composition (Bergstrom et al., 2007; Kirchstetter and Thatcher, 2012; Moosmüller et al., 2011; Schuster et al., 2006). Therefore the AAE of the aerosol can be used to differentiate between different sources of aerosols, due to the differences in chemical composition that has an influence on aerosol light absorption properties (e.g.

AMTD
7, 9733–9769, 2014

Andreae and Gelencser, 2006; Hoffer et al., 2006; Kirchstetter and Thatcher, 2012; Kirchstetter et al., 2004). The chemical composition of the absorbing aerosol does not exclusively determine the AAE, since a non or weakly absorbing coating can change the AAE of the aerosol (Gyawali et al., 2009; Lack and Cappa, 2010). However, AAEs have been used to distinguish between urban air pollution from biomass smoke (Clarke et al., 2007) and mineral dust events (Collaud Coen et al., 2004; Petzold et al., 2009). The spectral selectivity of absorption has also been used to estimate the contribution of absorption by OC in the aerosol (Kirchstetter and Thatcher, 2012).

Filter-based absorption measurement techniques are suitable for unattended use and are therefore widely used for measuring σ_{AP} and AAE of the aerosol. However, filter-based absorption measurements suffer from undesired and inevitable interaction between the deposited sample and the optical characteristics of the filter (Collaud Coen et al., 2010). These artifacts constantly change as a pristine filter gradually becomes so aerosol-laden and has to be changed.

Collimated light incident on the filter is subject to multiple scattering by the fibres in the filter. Consequently, the degree of collimation decreases as light penetrates into the filter. Therefore, the optical path length through the filter will increase and thus enhance light absorption by the sample embedded in the filter. The deposition of light scattering aerosols can also increase the optical path of the filter, and further enhance light absorption by the sample. In contrast, light absorbing particles will reduce the optical path length. Light absorbing aerosol particles are primarily responsible for the reduction of light transmittance through the filter. Several studies have focused on minimising these artifacts empirically with correction algorithms or correction functions (e.g. Bond et al., 1999; Collaud Coen et al., 2010; Müller et al., 2013; Ogren, 2010; Petzold and Schönlinner, 2004; Virkkula et al., 2005). An essential part of these corrections is to compensate for the influence of the filter on the deposited sample that changes with the filter transmittance (Tr), which is referred to as the filter loading correction function $f(\mathrm{Tr})$.

AMTD
7, 9733–9769, 2014

The need to use a filter loading correction function is well established. However, the influence of correction algorithms on the AAE has not been evaluated. The main objective of this study is to evaluate uncertainties involved with calculating AAE from σ_{AP} measured with filter-based measurement techniques that depend on correction algorithms. These uncertainties will also impinge on the assessment of the contribution of organics to light absorption. This study will focus specifically on the correction functions used for the Particle Soot Absorption Photometer (PSAP). Data gathered on the central Highveld in Sout Africa during the EUCAARI project (Laakso et al., 2012) was utilised. In addition to the primary objective of this study, the performance of a dilution setup used for the PSAP to prolong filter change time will be evaluated by comparing the diluted PSAP with a non-diluted Multi-Angle Absorption Photometer (MAAP).

2 Methods and measurements

2.1 Measurement site

The data used in this study comprise 23 months of measurements conducted at Elandsfontein on the central Highveld in South Africa from February 2009 to January 2011. A study by Laakso et al. (2012) already provides a comprehensive overview of the site; hence the description of the site is brief.

Figure 1 depicts the location of the Elandsfontein measurement station (26°14′43″ S, 29°25′30″ E). The station is located on the South African Highveld, which is an inland plateau that covers approximately 30 % of the surface area of South Africa. The site was located 1750 m above mean sea level (a.m.s.l.), with surrounding areas that range from 1400 to 1600 m a.m.s.l. (Laakso et al., 2012). Elandsfontein is within the Mpumalanga Province with a variety of industrial activities, which include 9 coal-fired power plants, a petrochemical plant and various pyrometallurgical smelters. In addition, other anthropogenic sources include trafific emissions and domestic combustion for heating and cooking. The densely populated Gauteng Province is located west of

AMTD
7, 9733–9769, 2014

Elandsfontein where the Johannesburg and Pretoria conurbation is situated (~ 140 km from Elandsfontein), as well as other industrial regions. A more detailed description of the site and a synopsis of meteorological conditions are presented by Laakso et al. (2012), and references therein.

2.2 Instruments

The instruments were connected to a Rupprecht & Patashnick PM_{10} inlet and the sample aerosol was dried using a self regenerating Silica gel drier (Tuch et al., 2009). In addition to the 3λ PSAP (Radiance Research, Seattle) and the MAAP (Model 5012, Thermo Scientific), a three-wavelength Nephelometer (Aurora 3000, Ecotech) was used to measure σ_{SP}. All measurements were converted to STP conditions (0 °C and 1013 hPa). The scattering coefficients were additionally corrected for truncation according to Müller et al. (2011a) and interpolated to the PSAP wavelengths.

The PSAP filters are changed manually and this should be done before they get too heavily loaded. At background sites this is not a problem but at polluted sites such as Elandsfontein the filters may have to be changed several times a day. Due to logistical reasons, the sample flow was diluted using the setup depicted in Fig. 2 to prolong the need to change filters. The dilution was arranged by mixing the sample air flow with clean, filtered air. The flow made a loop from a Thomas membrane pump through a flow fluctuation dampening chamber to an absolute filter, to a mixing tube and back to the pump. The dilution flow was tracked by measuring the pressure drop over a constriction in the dilution loop. The flow rates of the dilution loop were checked manually on a regular basis.

AMTD
7, 9733–9769, 2014

2.3 Calculation methods

2.3.1 Preprocessing

The basics of the filter-based absorption measurements are straightforward whereas the samples interactions with the filter matrix are not (Müller et al., 2013). Aerosol particles in a known volume of air deposits onto a fibre filter as the sample passes through the filter. The deposition of particles onto the filter-matrix will decrease the transmittance of light through the filter. Beer's law states that the attenuation of light in a medium will decrease exponentially from the initial intensity (I_0) to the transmitted intensity (I_t) in a given path length. By choosing I_0 as the intensity transmitted by a pristine filter, the interaction with light by the filter itself will initially be avoided. Thus, the change in the transmittance yields the uncorrected absorption coefficient (σ_0) of the deposited aerosol. For subsequent measurements, σ_0 can be written as

$$\sigma_0 = \frac{A}{Q \cdot \Delta t} \ln\left(\frac{I_{t-\Delta t}}{I_t}\right). \quad (2)$$

In Eq. (2), the sample spot size (A), sample flow rate (Q), and the time elapsed Δt represents the length of the sample-air column drawn through the filter. A more detailed derivation of the equation has been derived, e.g., by Weingartner et al. (2003). There are several assumptions associated with Eq. (2), as pointed out by Moosmüller et al. (2009), which will result in artifacts. The correction for inherent systematic errors, such as spot size correction and flow calibration, should be done on σ_0; not at a later stage in the data post processing. The studies by Bond et al. (1999) and Ogren (2010) describe how to correct for systematic errors in more detail. In this work σ_0 was calculated from the PSAP raw data by integrating the signal and reference counts over one hour periods and not by averaging the 1 s absorption coefficients calculated by the instrument itself. This results in clearly lower noise and detection limits, as pointed out by Springston and Sedlacek (2007).

AMTD
7, 9733–9769, 2014

At this step the calculated σ_0 was that after the dilution, here $\sigma_{0,\mathrm{DIL}}$. The relationship between the $\sigma_{0,\mathrm{DIL}}$ and the actual absorption coefficient of the sample ($\sigma_{0,\mathrm{S}}$) entering the mixing tube prior to dilution is

$$\sigma_{0,\mathrm{S}} = \sigma_{0,\mathrm{DIL}} \left(1 + \frac{Q_{\mathrm{DIL}}}{Q_{\mathrm{S}}}\right), \tag{3}$$

where Q_{DIL} is the dilution flow and Q_{S} is the sample flow into the mixing tube. For clarity, the subscripts used in Eq. (3) are explicitly expressed here. If not explicitly stated otherwise then σ_0 refers to $\sigma_{0,\mathrm{S}}$.

The noise of $\sigma_{0,\mathrm{S}}$ the can be estimated using the propagation of uncertainty as follows.

$$\delta\sigma_{0,\mathrm{S}} = \sqrt{\sum_i \left(\frac{\partial\sigma_{0,\mathrm{S}}}{\partial x_i}\right)\delta x_i^2} \tag{4}$$

The relative uncertainty of $\delta\sigma_0/\sigma_{\mathrm{DIL}}$ can then be written, after some rearrangements, in terms of the Q_{DIL} and Q_{S}, and their uncertainties (δQ_{DIL} and δQ_{S}) as follows

$$\frac{\delta\sigma_{0,\mathrm{S}}}{\sigma_{0,\mathrm{S}}} = \frac{Q_{\mathrm{DIL}}}{Q_{\mathrm{S}} + Q_{\mathrm{DIL}}} \sqrt{\left(\frac{\delta Q_{\mathrm{DIL}}}{Q_{\mathrm{DIL}}}\right)^2 + \left(\frac{\delta Q_{\mathrm{S}}}{Q_{\mathrm{S}}}\right)^2}, \tag{5}$$

given that the uncertainty of the diluted sample ($\delta\sigma_{0,\mathrm{DIL}}$) is insignificant in comparison to δQ_{DIL} and δQ_{S}. For a integration time of one hour, used in the this, this certainly holds true since $\delta\sigma_{0,\mathrm{DIL}}$ is many orders of magnitude lower than the uncertainties of the dilution flows. Springston and Sedlacek (2007) gives the equation for $\delta\sigma_{0,\mathrm{DIL}}$ as $10^{(-0.60-1.31\cdot\log(\Delta t))}$.

The relative uncertainty using Eq. (5) was estimated to be ~ 0.039, using the following values (in litres per minute): $Q_{\mathrm{DIL}} = 10$, $Q_{\mathrm{S}} = 0.70$, $\delta Q_{\mathrm{DIL}} = 0.3$, and $\delta Q_{\mathrm{S}} = 0.02$. The

AMTD
7, 9733–9769, 2014

respective values represent the flow rates (Q_{DIL} and Q_S) and their standard deviation (δQ_{DIL} and δQ_S) calculated from the data set.

The dilution flow of the system was tracked by measuring the pressure drop over a constriction in the dilution loop and flows were checked manually on a regular basis. Data associated with significant deviations or fluctuations from the desired Q_{DIL} value were omitted.

2.3.2 Absorption coefficients and Ångström exponents

The actual absorption coefficient σ_{AP} is calculated by combining σ_0 with the scattering coefficients obtained from the nephelometer. There exist two widely used correction methods: the function originally presented by Bond et al. (1999) and the algorithm presented by Virkkula et al. (2005). These two will be used in the present paper. The constrained two-stream (CTS) radiative transfer algorithm presented by Müller et al. (2013) was not applied in this work.

The purpose of the correction algorithms are to compensate for interactions between the deposited sample onto the filter and the filter matrix. The method presented by Bond et al. (1999) was further clarified in the study by Ogren (2010). The correction functions of Bond et al. (1999) and Ogren (2010) (hereafter O2010) can be written as

$$\sigma_{AP} = f(\mathrm{Tr})\sigma_0 - s \cdot \sigma_{SP}. \quad (6)$$

were σ_{AP} is the corrected light absorption coefficient. The subtraction on the right hand side of the equation is the fraction s of light scattering coefficients (σ_{SP}) interpreted as absorption by the instrument; also called apparent absorption. The O2010 $f(\mathrm{Tr})$ function is calculated with the equation

$$f(\mathrm{Tr}) = (k_a\ \mathrm{Tr} + k_b)^{-1}. \quad (7)$$

The O2010 correction function has been characterised in the transmittance range of 0.7–1.0 (Bond et al., 1999).

AMTD
7, 9733–9769, 2014

Virkkula et al. (2005), hereafter refered to as V2010 due to a erratum by Virkkula (2010), modified the single wavelength PSAP to measure light absorption coefficients at three wavelengths (467, 530 and 660 nm). The V2010 algorithm differs from that of O2010 since it also takes the single-scattering albedo ($SSA = \sigma_{SP}/(\sigma_{SP} + \sigma_{AP})$) of the aerosol into account and uses a logarithmic loading correction function, which is

$$f(\mathrm{Tr}) = k_0 + k_1(h_0 + h_1 \mathrm{SSA}) \ln(\mathrm{Tr}). \quad (8)$$

The constants (k_0 and h_0) and coefficients (k_1 and h_1) in Eq. (8) are different for each of the instruments wavelength (Virkkula, 2010) but also average values of all wavelengths were reported which is also included in the analysis (hereafter V2010avg). The study also reported different values for s in Eq. (6) for the different wavelengths. In the second term on the right hand side of Eq. (8), h_0 and h_1 corrects for the cross-dependency between k_1 and SSA. Explicitly, the multiple scattering correction, inherently included in the function $f(\mathrm{Tr})$, depends on the SSA of the aerosol and the filter transmittance in the algorithm. The filter transmittance range of the V2010 correction was characterised in the range of 0.4–1.0 and thus the V2010 correction is defined for a wider filter transmittance range than the O2010. After calculating the absorption coefficients at the three PSAP wavelengths with the different methods the AAE was calculated both for σ_{AP} and σ_0 using Eq. (1).

In addition, AAE was also calculated from transmittances at the three PSAP wavelengths. The attenuation of light in the filter (ATN) was first calculated as

$$\mathrm{ATN}(\lambda) = -100 \ln(\mathrm{Tr}(\lambda)). \quad (9)$$

Next AAE of ATN was calculated using Eq. (1) by substituting $\sigma_i(\lambda)$ with $\mathrm{ATN}(\lambda)$. This was done to make the analyses as comparable as possible with the studies of Kirchstetter and Thatcher (2012) who took filter samples and analysed them using spectrometers in transmission mode to determine the AAE from $\mathrm{ATN}(\lambda)$. The AAE calculated from ATN are profoundly different since the ATN is not measured incrementally, as is the case for σ_0 and σ_{AP}. The AAE of ATN at a certain Tr is the result of all deposited particles onto the filter prior to a specific Tr value.

AMTD
7, 9733–9769, 2014

2.3.3 Estimation of the contribution of OC to absorption

AAEs can also be used to estimate the contribution of OC to aerosol light absorption (Kirchstetter and Thatcher, 2012). Light absorption by OC occurs at the lower end of the visible spectrum and in the UV-spectrum (Kirchstetter and Thatcher, 2012; Schnaiter et al., 2006). Since OC absorbs predominantly at short wavelengths the presence of OC will increase the AAE. BC, on the other hand, here attributed a AAE of of unity. By attributing all light absorption at 660 nm to BC one can extrapolate the absorption of BC to shorter wavelengths using the AAE of BC. The absorption of OC is then the difference between the measured absorption and the contribution to absorption absorption by BC as defined above. The work by Kirchstetter and Thatcher (2012) gives the equation for the contribution of OC to ATN (ATN_{OC}) as follows

$$ATN_{OC}(\lambda) = ATN(\lambda, AE) - ATN_{BC}(\lambda, AE = 1). \quad (10)$$

The same approach can further be extended to include σ_{ap} values derived from the correction algorithms. Equation (10) then becomes

$$\sigma_{AP,OC}(\lambda) = \sigma_{AP}(\lambda, AAE) - \sigma_{AP,BC}(\lambda, AAE = 1), \quad (11)$$

where $\sigma_{AP,OC}$ stands for the amount of light absorption by OC after subtracting the contribution to light absorption by BC ($\sigma_{AP,BC}$) with a AAE=1.

The fraction of filter attenuation due to OC at different wavelengths was then calculated using Eq. (11a)

$$f_{OC}(ATN) = \frac{ATN_{OC}(\lambda)}{ATN(\lambda)} \quad (12a)$$

$$f_{OC}(abs) = \frac{\sigma_{ap,OC}(\lambda)}{\sigma_{ap}(\lambda)} \quad (12b)$$

as given by Kirchstetter and Thatcher (2012). To extend this approach to light absorption measurements using the different correction algorithms ATN_{OC} in Eq. (11) was substituted with $\sigma_{AP,OC}$ and ATN with σ_{AP} resulting in Eq. (12b).

AMTD
7, 9733–9769, 2014

2.3.4 MAAP data processing

The MAAP was used in the study as a reference to the diluted PSAP. However, the MAAP cannot be considered to be a true reference because it is also a filter-based measurement technique. The reference instrument should ideally retrieve light absorption coefficient from suspended particles, such as scattering minus extinction or photoacoustic light-absorption measurements (e.g., Lack et al., 2006). However, these instruments were not available in the present study. The MAAP is a single wavelength instrument (637 nm, Müller et al., 2011b) which uses a different approach to compensate for the artifacts associated with filter-based absorption methods (Petzold et al., 2005; Petzold and Schönlinner 2004). Furthermore, the instrument differs from the PSAP because it changes filters automatically using a filter tape. The output of the instrument is equivalent black carbon (BCe). This was converted back to σ_{AP} from

$$\sigma_{AP} = MAC \cdot BCe, \quad (13)$$

using mass absorption cross seciton of $6.6\,m^2\,g^{-1}$. A recent study by Hyvärinen et al. (2013) showed that the MAAP exhibits a filter change artefact at high BCe concentrations. The occurrence of the artefact depends on the rate of accumulation of BCe on the filter tape and thus decreasing MAAP sample flow rate will decrease the number of filter change artefacts in MAAP. At Elandsfontein the MAAP was operated at a 10 LPM flow rate. These periods were corrected according to the Hyvärinen et al. (2013) algorithm which lead to a change of −0.6 ‰ in σ_{AP} for all the data.

3 Results and discussion

3.1 Comparing the diluted PSAP with the non-diluted MAAP

The performance of the diluted PSAP was evaluated by comparison to the MAAP. The PSAP data were interpolated to the MAAP wavelength 637 nm by using the AAEs

AMTD
7, 9733–9769, 2014

obtained from the different algorithms. The respective relationships are shown in Fig. 3. The figure is based on PSAP data with a filter transmittance range of 0.7–1.0 (upper panel) and 0.4–0.7 (lower panel) for the V2010 and V2010avg correction algorithms, and the O2010 correction function. In the data set, 36 % of the data were in the Tr of 0.4–0.7 and 52 % in the range of 0.7–1.0. The average filter change interval during the measurement period was 10 days that amounted to a total of 70 filter changes. On average, Tr had decreased to 0.54 (ranging from a maxima Tr of 0.99 to a minima of 0.21) before it was changed. The dilution factor $(1 + D_{DIL}/Q_S)$ directly affects how often the filter needs to be changed. Thus, over 1000 filter changes could be reduced to 70 by diluting the sample.

The colour scale in the Fig. 3 represents the number of data points at a given grid point. Since both instruments are associated with uncertainties, the linear regression shown in the figure was calculated using the bivariate method of Williamson–York (Cantrell, 2008; York et al., 2004). The data was weighted by the inverse value of the maximum value of each data pair. The maximum value of the data points was chosen for weighing because the signal needs to be weighed, not the noise. Thus, large values are given a lower weight which otherwise tend to dictate the slope of the regression. Figure 3 shows that the MAAP consistently showed higher σ_{AP} values than the PSAP in the Tr range of 0.7–1.0 (upper panel). The slopes (and standard deviation) of the linear regression for that Tr range are 0.83 (± 0.28), 0.92 (± 0.30), and 0.90 (± 0.30) for the V2010, O2010 and V2010avg fits. In the Tr range of 0.4–0.7 (lower panel) the slopes are 0.95 (± 0.35), 0.94 (± 0.29), and 1.02 (± 0.29) for the V2010, O2010 and V2010avg fits. The standard deviations (std) were calculated from the standard error (se) of the fits as $\text{std} = \text{se} \cdot \sqrt{n}$.

The coefficients of determination (R^2) for the different corrections in comparison to the MAAP were, in the Tr range of 0.7–1.0, 0.89, 0.90 and 0.89 for the V2010, O2010, and V2010avg corrections. For the Tr range of 0.4–0.7, R^2 did not significantly change in comparison to the Tr range of 0.7–1.0. In the lower Tr range of 0.4–0.7 the R^2 values were 0.87 (V2010), 0.91 (O2010), and 0.86 (V2010avg).

AMTD
7, 9733–9769, 2014

Because the filter transmission correction functions differ, the σ_{AP} values should also be different. The difference should be a function of Tr. The values calculated using the V2010, V2010avg, and O2010 corrections were compared to the values measured with the MAAP (Fig. 4a), at 637 nm wavelength. It is evident that the V2010 correction gave lower values than the O2010 correction in the Tr range of 0.6–1.0. When Tr dropped below 0.6, the relationship was opposite which is in agreement with Virkkula (2010). The V2010avg and O2010 corrections yielded similar values at high Tr values which also contained the most number of data points (Fig. 4b). Figure 4a is in agreement with the regression slopes presented in Fig. 3. In the Tr range of 0.7–1.0, in Fig. 4a, the σ_{AP} values calculated using the V2010 correction are below the O2010 and V2010avg curves. This is reflected in the slope of the regression in the upper panel of Fig. 3. At a Tr of 0.6 there is a crossover between the V2010 correction yielding lower values than the O2010. Below a Tr of 0.6 the V2010 correction yielded higher values than the O2010 correction. For the whole Tr range of 0.4–0.7 both the V2010 and O2010 similar slope which is due to the crossover between the corrections at a Tr of 0.6.

3.2 Correction algorithms impact AAE

The difference between the correction algorithms was investigated further by calculating the AAEs of the aerosol using different corrections algorithms for the same data set. The analysis showed that the use of different corrections algorithms yield very different AAEs. Figure 5 presents the average AAE as a function of Tr for the V2010, V2010avg correction algorithms and for the O2010 correction function. Furthermore, σ_0 was included in the figure as a reference, which represents the AAE without any correction applied.

Figure 5 shows data from the Elandsfontein site and for a comparison AAEs calculated from PSAP data measured in a very different environment, the New England Air Quality Study (NEAQS) onboard the NOAA research ship Ronald Brown during Jul and Aug of 2002, off the east coast of the United States. The NEAQS data are those

AMTD
7, 9733–9769, 2014

presented by Virkkula et al. (2005) but here the AAEs were calculated with the V2010 values for the respective corrections.

There are common features in the two data sets. First, Fig. 5a and b depict that the AAE is largely dependent on the correction used. Second, the AAE is, however to a lesser extent, dependent on Tr, and to which degree seems to depend on the type of aerosol. Also shown in Fig. 5 is the AAE calculated from the wavelength-dependent ATN (Eq. 9). The filter correction algorithms and functions aim to compensate for the pre-deposited aerosol and incrementally derive the light absorption. This is argued to be the reason for the different shape of the AAE curve of ATN in Fig. 5 in comparison to σ_{AP}. The use of ATN to calculate AAEs will in both cases show consistently lower AAE values than those calculated from σ_{AP} using different correction schemes.

The average AAEs calculated from the Elandsfontein data using different corrections are summarised in Table 1. It should be emphasised that the number of data points decreases with the Tr, which will ensue in averages that do not equally represent the whole Tr range since more data are exists at high Tr values.

At Elandsfontein AAEs are obviously higher than during the NEAQS campaign. In both data sets the wavelength-dependent V2010 correction leads to the highest AAE. For the NEAQS data V2010 results in average AAE of 1.25, slightly higher than the 1.19 presented in Virkkula et al. (2005), but all other corrections and σ_0 yield AAEs < 1 (Fig. 5b). The AAEs that are below unit do not, however, imply that the corrections yield unphysical AAEs. Core/shell simulations have shown that a weakly or non-absorbing shell surrounding a BC core can lower the AAEs of particles significantly below unity (Gyawali et al., 2009; Lack and Cappa, 2010). The study by Gyawali et al. (2009) pointed out that care should be taken when drawing conclusions about the origin of the aerosol due to different AAEs depending on the core thickness surrounding the absorbing core.

Figure 5a shows that at Elandsfontein the AAEs derived from σ_{AP} calculated with the different corrections, although they yield different AAEs, do not greatly depend on Tr between 0.7 and 1.0, whereas the AAEs calculated from σ_0 and ATN have a clear

AMTD
7, 9733–9769, 2014

Tr dependency, they decrease with decreasing Tr. On the contrary, when Tr decreases below 0.7 the AAEs calculated from σ_{AP} with the different algorithms increase with decreasing Tr. Moreover, in the marine data (Fig. 5b) there is not an increase in AAE when the Tr drops below 0.7 as at Elandsfontein (Fig. 5a). This suggests that different aerosol types will impact the performance of the respective corrections.

Laboratory studies have shown that liquid non-absorbing secondary organic aerosol (SOA) can change the radiative transfer of light and the optical path of the fibre filter significantly (Cappa et al., 2008). Moreover, Cappa et al. (2008) showed that semi-volatile SOA can condense and evaporate from the filtre and chan thus change the liquid SOA coating of the fibre filters over time and thus impact the instrument response significantly. A study by Lack et al. (2008) showed that the effect can be significant even at low concentrations of SOA. However, the changes in absolute values σ_{AP} as reported by Cappa et al. (2008) when SOA concentrations change rapidly is likely to be dampened by the dilution flow arrangements in the this study. The absolute filtre of the setup in the dilution loop will likely dampen abrupt changes in the SOA concentration in the sampling line due to the large surface area of the filtre from which SOA partition between gas phase and liquid phase. It should be acknowledged that a buildup of liquid SOA onto the filtre can change the radiative transfer of light through the filtre and the extent of the wavelength dependence of the bias remains unknown. Under large SOA loadings the wavelength dependence of SOA soaked fibres in the filtre could potentially change the wavelength dependence of multiple scattering inside the filtre. This effect could also change the AAEs dependence on how deeply the pre-deposited particles have been embedded into the filtre (Lack et al., 2009; Nakayama et al., 2010).

The absolute change in AAEs as a function of Tr for the different data sets suggests that the praxis to change filters at a certain Tr will affect the AAEs of the data. For the Elandsfontein data, the median AAEs of Fig. 5, changed by 0.04 (V2010), −0.13 (O2010), −0.04 (V2010avg), −0.32 (σ_0), and −0.13 (ATN) when the Tr dropped from 1.0–0.7. For the marine NEAQS 2002 data, the AAEs changed by −0.06 (V2010), −0.10 (O2010), −0.03 (V2010avg), −0.22 (σ_0), and −0.07 (ATN) when Tr dropped

AMTD
7, 9733–9769, 2014

from 1.0–0.7. For both data sets, AAEs calculated from σ_0 and ATN experienced the greatest Tr dependency.

The AAEs from the wavelength-dependent V2010 algorithm are highest because all the constants in the algorithm are wavelength dependent. On the contrary, it is not that obvious why the non-wavelength-dependent methods do not yield the same AAEs. For instance, for the Elandsfontein data the V2010avg correction algorithm yielded higher AAEs than the O2010 correction function; as opposed to the behaviour of the NEAQS data set (Fig. 5). Moreover, the AAEs of σ_0 were consistently lower than those calculated from σ_{AP} using different corrections at Elandsfontein (Fig. 5a), whereas the AAEs of σ_0 was for the most part greater than the AAEs calculated using the V2010avg and O2010 corrections during NEAQS (Fig. 5b). The order of the AAEs in the non-wavelength-dependent corrections (O2010 and V2010avg) is argued to be a result of different scattering Ångström exponent (SAE) of the aerosol. The corrections depend on the scattering coefficients so it is reasonable that the wavelength dependency of scattering also has an effect on AAE. The average SAE was 1.55 at Elandsfontein whereas the SAE of the NEAQS 2002 aerosol was considerably higher, between 2 and 3 (Virkkula et al., 2005). This suggests that the size of the particles at Elandsfontein were larger than those measured during the NEAQS 2002 campaign.

The AAE dependence on the SAE of the aerosol for the V2010avg and O2010 corrections and the AAE calculated from σ_0 was analysed by making a simple simulation. σ_0 at $\lambda = 530$ nm was set to $10\,\mathrm{M\,m^{-1}}$ and AAE(σ_0) = 1 and the transmittances at the same wavelength to 0.96 and 0.62, representing two ranges of filter loading. The above σ_0 and Tr values were taken from real data measured at Elandsfontein, the AAE(σ_0) was set. The corrections were calculated for a case with low $\sigma_{SP} = 20\,\mathrm{M\,m^{-1}}$ at the nephelometer wavelength $\lambda = 550$ nm representing a aerosol with a low SSA and for a case representing a high SSA ($\sigma_{SP} = 100\,\mathrm{M\,m^{-1}}$); SAE was varied in the range 1–4 and the scattering coefficients were extrapolated to the PSAP wavelengths. The absorption coefficients were calculated using the V2010avg and O2010 algorithms and the AAEs from them.

AMTD
7, 9733–9769, 2014

The results of the simulation are shown in Fig. 6. Figure 6a shows that the scattering correction results in a different AAE than that calculated from the non-scattering corrected σ_0 even though the correction itself is not wavelength dependent. The figure also shows that the effect on AAE depends on Tr, scattering properties of the aerosol (σ_{SP} and SAE) and SSA. The impact is not as dramatic for the case with a low SSA since the scattering correction is consequently less in comparison to the case with high SSA values.

When comparing the AAEs calculated using the V2010avg algorithm and O2010 function in the same manner, the difference between the AAEs calculated using these corrections are not the same. Figure 6b that for different aerosol types (either a high or a low SSA and a range of SAE values) the corrections can yield a very different AAE. Moreover, the crossover when one correction yields a higher AAE than the other appears to depend on the filter Tr. Thus, the different behaviour of the V2010avg and O2010 corrections with respect to each other, and in comparison to σ_0 can be explained by the different type of aerosol between the sites. The analysis was restricted to V2010avg and O2010 only since V2010 consistently showed larger AAE values than the other corrections.

3.3 AAE as a function of SSA

The surface plots in Fig. 7 present the correlation between the AAE and the SSA. The figures were smoothened using a 3×3 matrix with equal weights for the surrounding grid points to make the interpretation of the figure more clear. The grid interval in the figure is 0.004 on the x-axis and 0.05 on the y-axis. The SSA of the aerosols was calculated by using the MAAP and the Nephelometer (interpolated to a 637 nm wavelength) data in order to make the comparison between the different corrections consistent, i.e. AAEs using different corrections will thus get the same SSA regardless of the correction used. Figure 7 shows again that the different corrections were prone to yield higher AAEs than when calculated directly from σ_0.

AMTD
7, 9733–9769, 2014

In the first column, distinct differences are observed when comparing the AAEs calculated using σ_{AP} from the V2010, V2010avg, and O2010 corrections, and σ_0. The AAEs of σ_0 were mostly in the range of 0.84–1.50. AAEs calculated with the V2010 correction were mostly in the range of 1.52–2.40, whereas the V2010avg correction yielded AAEs in the range of 1.01–1.85. AAEs calculated with the O2010 correction were in the range of 0.95–1.73. It should be noted that the O2010 correction only include data that were measured at a Tr above 0.7, while the V2010avg and V20 10 corrections that included data with a Tr above 0.4.

The second and third column of Fig. 7 depicts that the most frequently occurring range in AAE and SSA did not always coincide with the highest σ_{AP} and σ_{SP} values. The high σ_{AP} values, were for the most part observed outside of the most frequently occurring combination of SSA and AAE values. However, high σ_{AP} values were associated with a lower SSA suggesting that the aerosol was not long range transported biomass burning smoke. Furthermore, high values of σ_{SP} also did not fall into the most frequently occurring combination of SSA and AAE at the site. The areas that show the highest σ_{AP} values are not the coordinates that are associated with the highest σ_{SP} values, which suggest different sources.

All corrections assume that the apparent absorption is a certain fraction of the σ_{SP}. A high SSA combined with high σ_{SP} seems to scatter events throughout the AAE axis depending on the correction used; by how much is likely to be affected by the state of the filter when the event occurred. In other words, the different corrections are prone towards different AAEs given that the SSA and σ_{SP} are high, which is in agreement with Fig. 6.

3.4 Corrections' impact OC estimation

The AAEs were next used for estimating the contribution of OC to aerosol light absorption as described in Sect. 2.3.3. Figure 8 underlines the differencies between corrections algorithms, functions and different approaches when AAEs are used to estimate the amount of absorption by OC. Figure 8a depicts the absorption attributed to BC with

AMTD
7, 9733–9769, 2014

respect to the total absorption by the aerosol used in Eqs. (10) and (11) using the AAE values in Table 1 in the Tr range of 0.7–1.0.

The figure shows the f_{OC} (abs) and f_{OC} (ATN) as a function of wavelength for the different correction algorithms. From the figure it is evident that there is a significant difference in the calculated f_{OC} by using AAE using based on different correction schemes. The correction function that gives the highest AAE also predicts the highest contribution of absorption by OC. The f_{OC} calculated using AAE with the V2010 correction was a factor of approximately 3 higher than if f_{OC} was calculated from the non-corrected σ_0. Moreover, the f_{OC} of the V2010avg and O2010 corrections were roughly 38 % and 63 % larger than if no correction was used.

As discussed earlier, f_{OC} (abs) are based on subsequent measurements using the same filter whereas the f_{OC} (ATN) can be considered to be one long measurement until Tr has dropped to a certain value. In the study by Kirchstetter and Thatcher (2012) the ATN ranged between 2 and 23 for most of the samples. That is equivalent to a Tr ranging between 0.98 and 0.79, see Eq. (9). In this study, the average Tr of the filter (in the Tr range of 0.7–1.0) was 0.86. Thus, the study of Kirchstetter and Thatcher (2012) was not entirely different in terms of filter loadings than this study. When comparing f_{OC} (ATN) to $f_{OC}(\sigma_0)$, f_{OC} (ATN) was 17 % higher than $f_{OC}(\sigma_0)$. This relationship, however, depends on the type of aerosol and the Tr of the filters (Fig. 5).

4 Conclusions

The study showed a means by which the sample air of the PSAP can be diluted. After a dilution of 1 : 14 the correlation between the diluted PSAP and a non-diluted MAAP was good after post processing the PSAP data to a temporal resolution of one hour. The correlation coefficients between the absorption coefficients were approximately 0.9 and the bivariate regression slopes were between 0.83 and 0.92 depending on the correction algorithm used. The extent of the dilution of the sampled air extends the need to change filters in the PSAP expand the applicability of the instrument to stations

AMTD
7, 9733–9769, 2014

to remote areas or areas that suffer from high levels of pollution, without significantly compromising data quality or introduce noise. A further improvement of the dilution arrangement could be to have an mass-flow controller for the dilution flow to provide more accurate data for the dilution calculations.

The AAEs calculated from the data showed a large dependency on the algorithm used to convert the uncorrected "raw" absorption coefficient σ_0 to the aerosol absorption coefficient σ_{AP}. The study showed that the correction algorithms used for PSAP measurements can lead to conflicting conclusions about aerosols using the same data. Depending on the algorithm used to calculate the AAE, the average AAE of aerosols varied between 1.33 and 1.96. The lower value suggests urban pollution and the higher suggests biomass burning aerosols.

The highest AAEs at Elandsfontein were obtained from the σ_{AP} calculated with the wavelength-dependent V2010 algorithm and the lowest from the σ_0. When the AAEs were calculated from a marine aerosol data the order changed: again the V2010 algorithm yielded the highest values but the lowest ones were obtained from σ_{AP} calculated with non-wavelength-dependent algorithms. The fact that the wavelength-dependent V2010 algorithm yields highest AAEs depends on the wavelength dependency of both the loading correction and the scattering correction within it. It cannot be determined from this analysis which of them is the true one but some evaluation can be made. If an algorithm for calculating σ_{ap} from σ_0 worked perfectly at all transmittances (Tr) the AAE should not depend on Tr. With this criterium the AAE calculated directly from σ_0 is not good because it decreased clearly with decreasing Tr. Also the AAE calculated directly from the Tr decreased with a decreasing Tr, even though less than that calculated from σ_0. The conclusion is that spectral attenuation measurements from filter samples may yield lower AAE values when the filters are heavily loaded than when the amount of aerosol is light.

The uncertainties in AAEs calculated using different correction algorithms can be as significant as the thickness of the shell that can encapsulate an absorbing BC core. Thus, in the quest to distinguish between urban pollution and biomass burning type

AMTD
7, 9733–9769, 2014

aerosol one should also consider the influence of the correction used and the uncertainties associated with them.

Furthermore, the difference in AAEs can also result in large differences when estimating the contribution of OC to light absorption. Depending on the algorithm used in this study, the estimated fraction of absorption by OC ranged between 0.27 and 0.11 at a wavelength of 467 nm. Moreover, if no correction function was used for the data the OC fraction was even lower (0.08).

Ideally, AAEs should be determined with multi-wavelength absorption measurements on the aerosol while the aerosol is still suspended, such as with photoacoustic measurements or the extinction minus scattering method. This method would be a valuable tool for characterising how the correction algorithms perform at different sites at multiple wavelengths. The study would need to include the deposition of liquid SOA to determine how the radiative transfer at multiple wavelengths would affect the AAEs in a similar manner that was conducted by Lack et al. (2008) at multiple wavelengths.

Acknowledgements. The project was funded by the European commission 6th Framework programme project EUCAARI. The authors greatly acknowledge the Academy of Finland Centre of Excellence program (project no. 1118615 and 272041). Eskom and Sasol Ltd. are acknowledged for logistical, financial and on-site support.

References

Amante, C. and Eakins, B. W.: ETOPO1 1 Arc-Minute Global Relief Model: Procedures, Data Sources and Analysis, NOAA Technical Memorandum NESDIS NGDC-24, 19 March, 2009.

Andreae, M. O. and Gelencsér, A.: Black carbon or brown carbon? The nature of light-absorbing carbonaceous aerosols, Atmos. Chem. Phys., 6, 3131–3148, doi:10.5194/acp-6-3131-2006, 2006.

Bergstrom, R. W., Pilewskie, P., Russell, P. B., Redemann, J., Bond, T. C., Quinn, P. K., and Sierau, B.: Spectral absorption properties of atmospheric aerosols, Atmos. Chem. Phys., 7, 5937–5943, doi:10.5194/acp-7-5937-2007, 2007.

AMTD
7, 9733–9769, 2014

Bond, T. C., Anderson, T. L., and Campbell, D.: Calibration and intercomparison of filter-based measurements of visible light absorption by aerosols, Aerosol Sci. Tech., 30, 582–600, 1999.
Bond, T. C., Doherty, S. J., Fahey, D. W., Forster, P. M., Berntsen, T., DeAngelo, B. J., Flanner, M. G., Ghan, S., Kärcher, B., Koch, D., Kinne, S., Kondo, Y., Quinn, P. K., Sarofim, M. C., Schultz, M. G., Schulz, M., Venkataraman, C., Zhang, H., Zhang, S., Bellouin, N., Guttikunda, S. K., Hopke, P. K., Jacobson, M. Z., Kaiser, J. W., Klimont, Z., Lohmann, U., Schwarz, J. P., Shindell, D., Storelvmo, T., Warren, S. G., and Zender, C. S.: Bounding the role of black carbon in the climate system: a scientific assessment, J. Geophys. Res.-Atmos., 118, 5380–5552, doi:10.1002/jgrd.50171, 2013.
Cantrell, C. A.: Technical Note: Review of methods for linear least-squares fitting of data and application to atmospheric chemistry problems, Atmos. Chem. Phys., 8, 5477–5487, doi:10.5194/acp-8-5477-2008, 2008.
Cappa, C. D., Lack, D. A., Burkholder, J. B., and Ravishankara, A. R.: Bias in filter-based aerosol light absorption measurements due to organic aerosol loading: evidence from laboratory measurements, Aerosol Sci. Tech., 42, 1022–1032, doi:10.1080/02786820802389285, 2008.
Clarke, A., McNaughton, C., Kapustin, V., Shinozuka, Y., Howell, S., Dibb, J., Zhou, J., Anderson, B., Brekhovskikh, V., Turner, H., and Pinkerton, M.: Biomass burning and pollution aerosol over North America: organic components and their influence on spectral optical properties and humidification response, J. Geophys. Res.-Atmos., 112, D12S18, doi:10.1029/2006JD007777, 2007.
Collaud Coen, M., Weingartner, E., Schaub, D., Hueglin, C., Corrigan, C., Henning, S., Schwikowski, M., and Baltensperger, U.: Saharan dust events at the Jungfraujoch: detection by wavelength dependence of the single scattering albedo and first climatology analysis, Atmos. Chem. Phys., 4, 2465–2480, doi:10.5194/acp-4-2465-2004, 2004.
Collaud Coen, M., Weingartner, E., Apituley, A., Ceburnis, D., Fierz-Schmidhauser, R., Flentje, H., Henzing, J. S., Jennings, S. G., Moerman, M., Petzold, A., Schmid, O., and Baltensperger, U.: Minimizing light absorption measurement artifacts of the Aethalometer: evaluation of five correction algorithms, Atmos. Meas. Tech., 3, 457–474, doi:10.5194/amt-3-457-2010, 2010.
Gyawali, M., Arnott, W. P., Lewis, K., and Moosmüller, H.: In situ aerosol optics in Reno, NV, USA during and after the summer 2008 California wildfires and the influence of absorbing

AMTD
7, 9733–9769, 2014

and non-absorbing organic coatings on spectral light absorption, Atmos. Chem. Phys., 9, 8007–8015, doi:10.5194/acp-9-8007-2009, 2009.
Haywood, J. and Boucher, O.: Estimates of the direct and indirect radiative forcing due to tropospheric aerosols: a review, Rev. Geophys., 38, 513–543, 2000.
Hoffer, A., Gelencsér, A., Guyon, P., Kiss, G., Schmid, O., Frank, G. P., Artaxo, P., and Andreae, M. O.: Optical properties of humic-like substances (HULIS) in biomass-burning aerosols, Atmos. Chem. Phys., 6, 3563–3570, doi:10.5194/acp-6-3563-2006, 2006.
Hyvärinen, A.-P., Vakkari, V., Laakso, L., Hooda, R. K., Sharma, V. P., Panwar, T. S., Beukes, J. P., van Zyl, P. G., Josipovic, M., Garland, R. M., Andreae, M. O., Pöschl, U., and Petzold, A.: Correction for a measurement artifact of the Multi-Angle Absorption Photometer (MAAP) at high black carbon mass concentration levels, Atmos. Meas. Tech., 6, 81–90, doi:10.5194/amt-6-81-2013, 2013.
Kirchstetter, T. W. and Thatcher, T. L.: Contribution of organic carbon to wood smoke particulate matter absorption of solar radiation, Atmos. Chem. Phys., 12, 6067–6072, doi:10.5194/acp-12-6067-2012, 2012.
Kirchstetter, T. W., Novakov, T., and Hobbs, P. V.: Evidence that the spectral dependence of light absorption by aerosols is affected by organic carbon, J. Geophys. Res.-Atmos., 109, D21208, doi:10.1029/2004JD004999, 2004.
Laakso, L., Vakkari, V., Virkkula, A., Laakso, H., Backman, J., Kulmala, M., Beukes, J. P., van Zyl, P. G., Tiitta, P., Josipovic, M., Pienaar, J. J., Chiloane, K., Gilardoni, S., Vignati, E., Wiedensohler, A., Tuch, T., Birmili, W., Piketh, S., Collett, K., Fourie, G. D., Komppula, M., Lihavainen, H., de Leeuw, G., and Kerminen, V.-M.: South African EUCAARI measurements: seasonal variation of trace gases and aerosol optical properties, Atmos. Chem. Phys., 12, 1847–1864, doi:10.5194/acp-12-1847-2012, 2012.
Lack, D. A. and Cappa, C. D.: Impact of brown and clear carbon on light absorption enhancement, single scatter albedo and absorption wavelength dependence of black carbon, Atmos. Chem. Phys., 10, 4207–4220, doi:10.5194/acp-10-4207-2010, 2010.
Lack, D. A., Lovejoy, E. R., Baynard, T., Pettersson, A., and Ravishankara, A. R.: Aerosol absorption measurement using photoacoustic spectroscopy: sensitivity, calibration, and uncertainty developments, Aerosol Sci. Tech., 40, 697–708, doi:10.1080/02786820600803917, 2006.
Lack, D. A., Cappa, C. D., Covert, D. S., Baynard, T., Massoli, P., Sierau, B., Bates, T. S., Quinn, P. K., Lovejoy, E. R., and Ravishankara, A. R.: Bias in filter-based aerosol light absorp-

AMTD
7, 9733–9769, 2014

tion measurements due to organic aerosol loading: evidence from ambient measurements, Aerosol Sci. Tech., 42, 1033–1041, doi:10.1080/02786820802389277, 2008.
Lack, D. A., Cappa, C. D., Cross, E. S., Massoli, P., Ahern, A. T., Davidovits, P., and Onasch, T. B.: Absorption enhancement of coated absorbing aerosols: validation of the photo-acoustic technique for measuring the enhancement, Aerosol Sci. Tech., 43, 1006–1012, doi:10.1080/02786820903117932, 2009.
Lohmann, U. and Feichter, J.: Global indirect aerosol effects: a review, Atmos. Chem. Phys., 5, 715–737, doi:10.5194/acp-5-715-2005, 2005.
Moosmüller, H., Chakrabarty, R. K., and Arnott, W. P.: Aerosol light absorption and its measurement: a review, J. Quant. Spectrosc. Ra., 110, 844–878, doi:10.1016/j.jqsrt.2009.02.035, 2009.
Moosmüller, H., Chakrabarty, R. K., Ehlers, K. M., and Arnott, W. P.: Absorption Ångström coefficient, brown carbon, and aerosols: basic concepts, bulk matter, and spherical particles, Atmos. Chem. Phys., 11, 1217–1225, doi:10.5194/acp-11-1217-2011, 2011.
Müller, T., Laborde, M., Kassell, G., and Wiedensohler, A.: Design and performance of a three-wavelength LED-based total scatter and backscatter integrating nephelometer, Atmos. Meas. Tech., 4, 1291–1303, doi:10.5194/amt-4-1291-2011, 2011a.
Müller, T., Henzing, J. S., de Leeuw, G., Wiedensohler, A., Alastuey, A., Angelov, H., Bizjak, M., Collaud Coen, M., Engström, J. E., Gruening, C., Hillamo, R., Hoffer, A., Imre, K., Ivanow, P., Jennings, G., Sun, J. Y., Kalivitis, N., Karlsson, H., Komppula, M., Laj, P., Li, S.-M., Lunder, C., Marinoni, A., Martins dos Santos, S., Moerman, M., Nowak, A., Ogren, J. A., Petzold, A., Pichon, J. M., Rodriquez, S., Sharma, S., Sheridan, P. J., Teinilä, K., Tuch, T., Viana, M., Virkkula, A., Weingartner, E., Wilhelm, R., and Wang, Y. Q.: Characterization and intercomparison of aerosol absorption photometers: result of two intercomparison workshops, Atmos. Meas. Tech., 4, 245–268, doi:10.5194/amt-4-245-2011, 2011b.
Müller, T., Virkkula, A., and Ogren, J. A.: Constrained two-stream algorithm for calculating aerosol light absorption coefficient from the Particle Soot Absorption Photometer, Atmos. Meas. Tech. Discuss., 6, 11093–11144, doi:10.5194/amtd-6-11093-2013, 2013.
Nakayama, T., Kondo, Y., Moteki, N., Sahu, L. K., Kinase, T., Kita, K., and Matsumi, Y.: Size-dependent correction factors for absorption measurements using filter-based photometers: PSAP and COSMOS, J. Aerosol Sci., 41, 333–343, doi:10.1016/j.jaerosci.2010.01.004, 2010.

AMTD
7, 9733–9769, 2014

Ogren, J. A.: Comment on "Calibration and intercomparison of filter-based measurements of visible light absorption by aerosols", Aerosol Sci. Tech., 44, 589–591, doi:10.1080/02786826.2010.482111, 2010.
Petzold, A. and Schönlinner, M.: Multi-angle absorption photometry – a new method for the measurement of aerosol light absorption and atmospheric black carbon, J. Aerosol Sci., 35, 421–441, doi:10.1016/j.jaerosci.2003.09.005, 2004.
Petzold, A., Schloesser, H., Sheridan, P. J., Arnott, W. P., Ogren, J. A., and Virkkula, A.: Evaluation of multiangle absorption photometry for measuring aerosol light absorption, Aerosol Sci. Tech., 39, 40–51, doi:10.1080/027868290901945, 2005.
Petzold, A., Rasp, K., Weinzierl, B., Esselborn, M., Hamburger, T., Dörnbrack, A., Kandler, K., Schütz, L., Knippertz, P., Fiebig, M., and Virkkula, A.: Saharan dust absorption and refractive index from aircraft-based observations during SAMUM 2006, Tellus B, 61, 118–130, doi:10.1111/j.1600-0889.2008.00383.x, 2009.
Schnaiter, M., Gimmler, M., Llamas, I., Linke, C., Jäger, C., and Mutschke, H.: Strong spectral dependence of light absorption by organic carbon particles formed by propane combustion, Atmos. Chem. Phys., 6, 2981–2990, doi:10.5194/acp-6-2981-2006, 2006.
Schuster, G., Dubovik, O., and Holben, B.: Angstrom exponent and bimodal aerosol size distributions, J. Geophys. Res.-Atmos., 111, D07207, doi:10.1029/2005JD006328, 2006.
Springston, S. R. and Sedlacek III, A. J.: Noise characteristics of an instrumental particle absorbance technique, Aerosol Sci. Tech., 41, 1110–1116, doi:10.1080/02786820701777457, 2007.
Tuch, T. M., Haudek, A., Müller, T., Nowak, A., Wex, H., and Wiedensohler, A.: Design and performance of an automatic regenerating adsorption aerosol dryer for continuous operation at monitoring sites, Atmos. Meas. Tech., 2, 417–422, doi:10.5194/amt-2-417-2009, 2009.
Virkkula, A.: Correction of the calibration of the 3-wavelength Particle Soot Absorption Photometer (3 PSAP), Aerosol Sci. Tech., 44, 706–712, doi:10.1080/02786826.2010.482110, 2010.
Virkkula, A., Ahlquist, N. C., Covert, D. S., Arnott, W. P., Sheridan, P. J., Quinn, P. K., and Coffman, D. J.: Modification, calibration and a field test of an instrument for measuring light absorption by particles, Aerosol Sci. Tech., 39, 68–83, doi:10.1080/027868290901963, 2005.
Weingartner, E., Saathoff, H., Schnaiter, M., Streit, N., Bitnar, B., and Baltensperger, U.: Absorption of light by soot particles: determination of the absorption coefficient by means of aethalometers, J. Aerosol Sci., 34, 1445–1463, doi:10.1016/S0021-8502(03)00359-8, 2003.

AMTD
7, 9733–9769, 2014

York, D., Evensen, N. M., Martinez, M. L., and Delgado, J. D. B.: Unified equations for the slope, intercept, and standard errors of the best straight line, Am. J. Phys., 72, 367–375, doi:10.1119/1.1632486, 2004.

AMTD
7, 9733–9769, 2014

Table 1. AEs calculated from the Elandsfontein data using different correction algorithms, σ_0, and ATN. The values in the parenthesises represent the AAE standard deviation.

Correction	AAE	
	0.4 < Tr < 1.0	0.7 < Tr < 1.0
V2010	1.96 (± 0.44)	1.90 (± 0.38)
V2010avg	1.43 (± 0.42)	1.39 (± 0.36)
O2010	1.34 (± 0.39)	1.33 (± 0.34)
σ_0	1.17 (± 0.33)	1.25 (± 0.29)
ATN	1.24 (± 0.17)	1.29 (± 0.18)

AMTD
7, 9733–9769, 2014

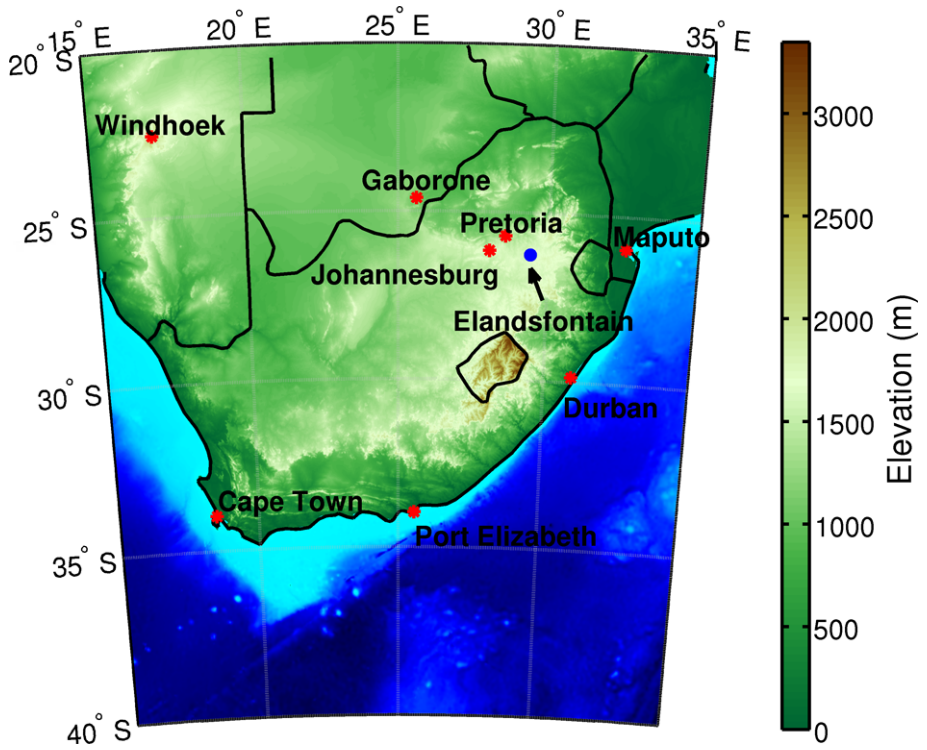

Figure 1. Map of South Africa and the location (26°14′43″ S, 29°25′30″ E) of the Elandsfontein measurement station on the South-African Highveld. The figure is based on the ETOPO1 bedrock data set (Amante and Eakins, 2009).

AMTD
7, 9733–9769, 2014

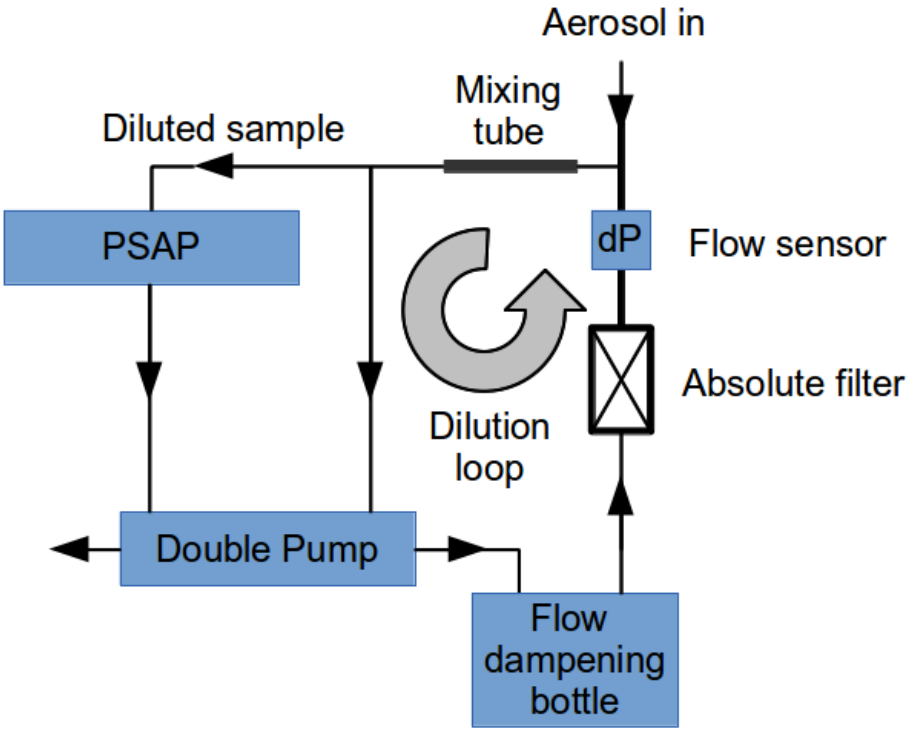

Figure 2. Simplified schematics of the sample air dilution loop used to prolong filter change intervals.

AMTD
7, 9733–9769, 2014

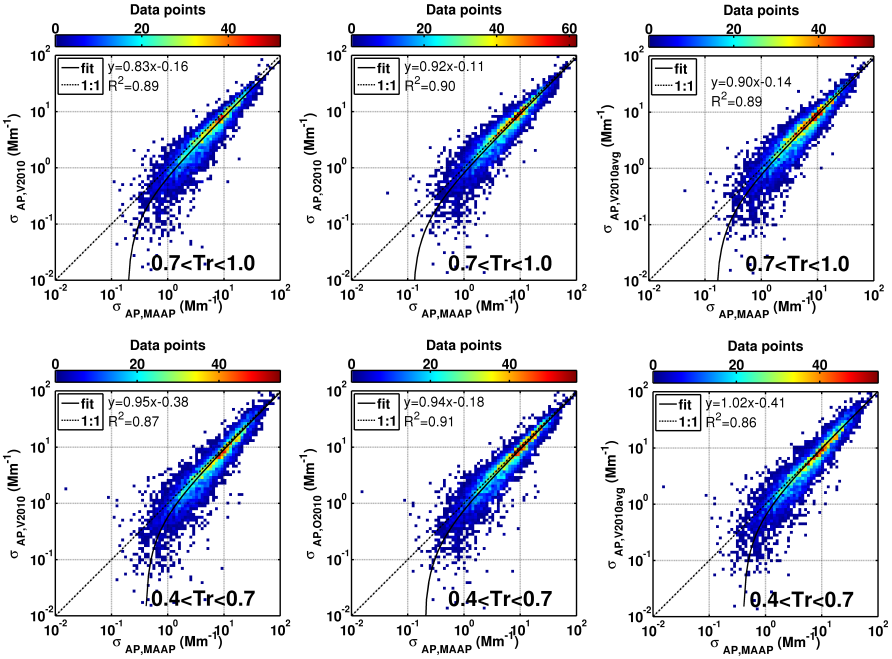

Figure 3. The relationship between light absorption coefficients measured by the MAAP ($\sigma_{AP,MAAP}$) and PSAP ($\sigma_{AP,V2010}$, $\sigma_{AP,O2010}$ and $\sigma_{AP,V2010avg}$), respectively. The upper and lower panels show data with a Tr range of 0.7–1.0 and 0.4–0.7, respectively. The integration time of the data plotted is one hour. The color legends indicate the number of data points in the scatter plot at a given coordinate. The linear regression was done using the bivariate method.

AMTD
7, 9733–9769, 2014

Different AAEs between correction algorithms for PASP

J. Backman et al.

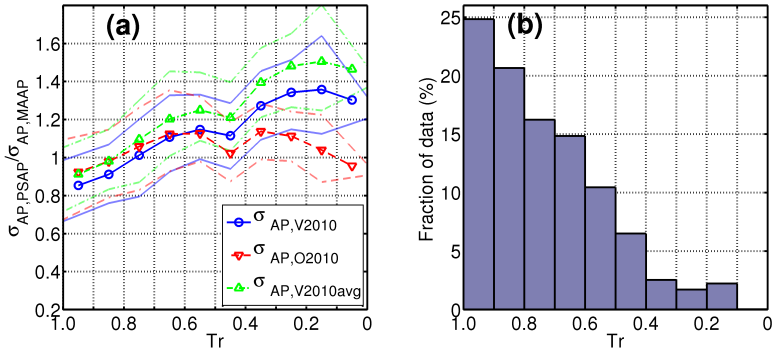

Figure 4. The influence of the PSAP's filter transmittance (Tr) on σ_{AP} in comparison to σ_{AP} from the MAAP and data coverage. **(a)** The median fraction of σ_{AP} calculated using the V2010 (blue), O2010 (red), and V2010avg (green) corrections in comparison to the MAAP ($\sigma_{AP,MAAP}$). The faden dashed lines represent the 25th and 75th percentile range with the legend color coding. **(b)** The percentage of data points for a given Tr range.

AMTD
7, 9733–9769, 2014

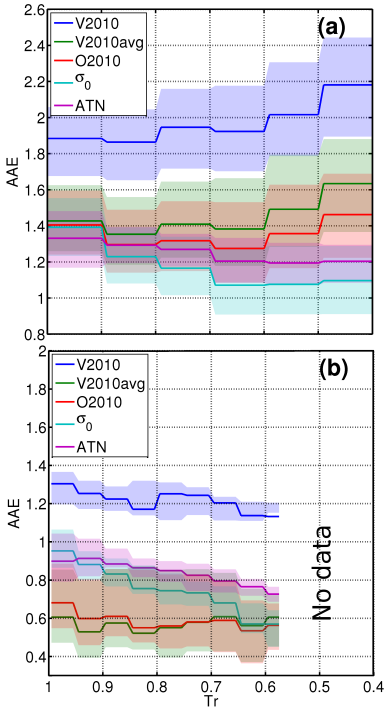

Figure 5. AAEs calculated using different correction algorithms, σ_0, and the AAEs calculated from ATN as a function of Tr. The solid lines represent the median AAE for the different corrections, σ_0 and ATN. The lines are ramped to indicate the Tr range the median was calculated from. The faded colored patches show the 25th to 75th percentile range of the AAEs lines with the same color. The panel **(a)** is based on Elandsfontein data and **(b)** is based on NEAQS 2002 campaign data. During the NEAQS 2002 campaign the filter was changed at higher filter transmittances than at Elandsfontein. Hence there is no data when Tr < 0.775

AMTD
7, 9733–9769, 2014

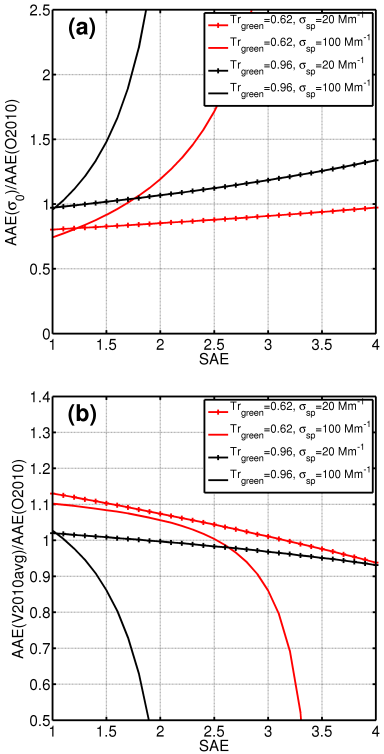

Figure 6. Simulation of the impact of SAE on the AAE calculated using different correction algorithms. The impact on the AAE was used assuming an AE of 1 when σ_0 was 10 M m^{-1} at 530 nm. The upper panel **(a)** shows the ratio between the AE of σ_0 and the AAE calculated using O2010 correction. The lower panel **(b)** shows the ratio between AAE derived using the V2010avg and the O2010 corrections.

AMTD
7, 9733–9769, 2014

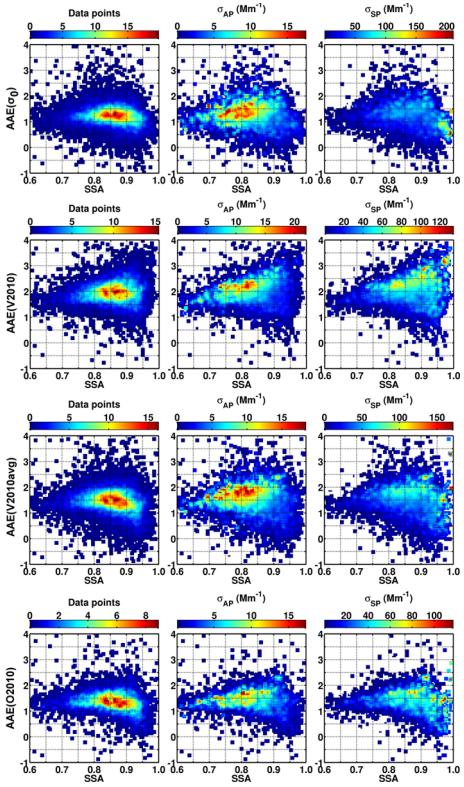

Figure 7. AAE as a function of SSA color coded with the number of data points σ_{AP}, and σ_{AP}. for the three corrections algorithms investigated and σ_0. The SSA was calculated using MAAP and Nephelometer data at 637 nm wavelength to fix the x scale for all subplots. Furthermore, MAAP data was used for σ_{AP} in the middle column. The AAE was calculated for σ_0 (first rows), V2010 (second row), V2010avg (third row), and for the O2010 (bottom row) correction.

AMTD
7, 9733–9769, 2014

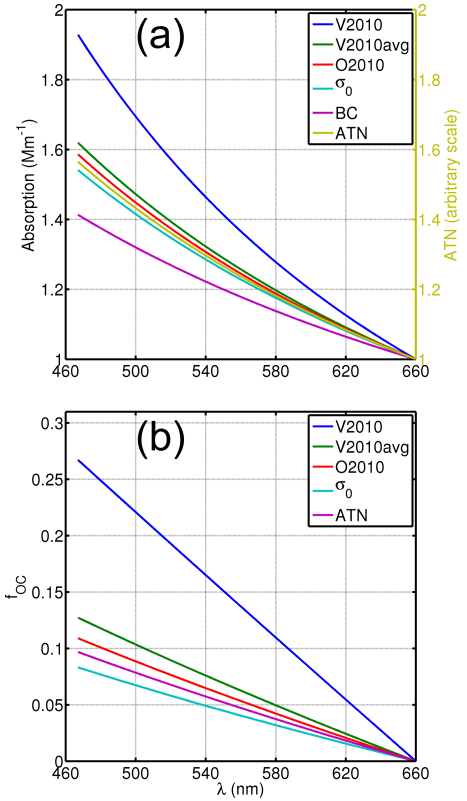

Figure 8. The difference in the wavelength dependency of absorption using different approaches for deriving AAEs and their impact on the estimated fraction of absorption by OC (f_{OC}). **(a)** The wavelength dependency of absorption and filter attenuation ATN calculated using the AAEs of Table 1. At 660 nm all absorption is attributed to BC with a AAE of unity. **(b)** The wavelength dependency of f_{OC} which is the fraction of absorption that exceeds the absorption of BC from Eqs. (12a) and (12b).

AMTD
7, 9733–9769, 2014